# Fatty acids metabolism affects the therapeutic effect of anti-PD-1/PD-L1 in tumor immune microenvironment in clear cell renal cell carcinoma

**Hansen Lin** ( linhs@mail2.sysu.edu.cn )
Sun Yat-sen University First Affiliated Hospital https://orcid.org/0000-0002-8289-6618
**Liangmin Fu**
Sun Yat-sen University First Affiliated Hospital
**Jiazheng Cao**
Jiangmen Central Hospital
**Zhenhua Chen**
Sun Yat-sen University First Affiliated Hospital https://orcid.org/0000-0002-8889-5122
**Jun Lu**
Sun Yat-sen University First Affiliated Hospital
**Lizhen Zhang**
Sun Yat-sen University First Affiliated Hospital
**Wei Chen**
Sun Yat-sen University First Affiliated Hospital
**Xiaofei Li**
Sun Yat-sen University First Affiliated Hospital
**Mukhtar Adan Mumin**
Sun Yat-sen University First Affiliated Hospital
**Gaosheng Yao**
Sun Yat-sen University First Affiliated Hospital
**Jiahao Bao**
Sun Yat-Sen University Guanghua School of Stomatology
**Yiqi Zhao**
Sun Yat-sen University Zhongshan School of Medicine
**Yujun Liu**
Sun Yat-sen University Zhongshan School of Medicine
**Jiangquan Zhu**
Sun Yat-sen University First Affiliated Hospital
**Yinghan Wang**
Sun Yat-sen University First Affiliated Hospital
**Guannan Shu**

Sun Yat-sen University First Affiliated Hospital

**Minyu Chen**

Sun Yat-sen University First Affiliated Hospital

**Junhang Luo**

Sun Yat-sen University First Affiliated Hospital

**Xinwei Zhou**

Sun Yat-sen University First Affiliated Hospital

**Yuhang Chen**

Sun Yat-sen University First Affiliated Hospital

**Pengju Li**

Sun Yat-sen University First Affiliated Hospital

**Quanhui Xu**

Sun Yat-sen University First Affiliated Hospital

---

**Research Article**

**Keywords:** fatty acids metabolism, clear cell renal cell carcinoma (ccRCC), tumor immune microenvironment, anti-PD-1/PD-L1 therapy

**Posted Date:** March 15th, 2023

**DOI:** https://doi.org/10.21203/rs.3.rs-2634233/v1



---

**Version of Record:** A version of this preprint was published at Journal of Translational Medicine on May 23rd, 2023. See the published version at https://doi.org/10.1186/s12967-023-04161-z.

# Abstract

**Background:** Clear cell renal cell carcinoma (ccRCC) is a highly invasive and metastatic subtype of kidney malignancy and is correlated with metabolic reprogramming for adaptation to the tumor microenvironment comprising infiltrated immune cells and immunomodulatory molecules. The role of immune cells in the tumor microenvironment (TME) and their association with abnormal fatty acids metabolism in ccRCC remain poorly understood.

**Method:** Data from TGCA-KIRC, E-MTAB-1980, CheckMate-025, IMmotion150 and IMmotion151 cohort were obtained for subsequent analysis. After differential expression genes identification, the signature was constructed through univariate Cox proportional hazard regression and simultaneously the least absolute shrinkage and selection operator (Lasso) analysis and the predictive performance of our signature was assessed by using receiver operating characteristic (ROC), Kaplan–Meier (KM) survival analysis, nomogram, drug sensitivity analysis, immunotherapeutic effect analysis and enrichment analysis. Immunohistochemistry (IHC), qPCR and western blot were performed to measure related mRNA or protein expression. Biological features were evaluated by wound healing, cell migration and invasion assays and colony formation test and analyzed using coculture assay and flow cytometry.

**Results:** Twenty fatty acids metabolism-related mRNA signatures were constructed in TCGA and possessed a strong predictive performance demonstrated through time-dependent ROC and KM survival analysis. Notably, the high-risk group exhibited an impaired response to anti-PD-1/ PD-L1(Programmed death-1 receptor/Programmed death-1 receptor-ligand) therapy compared to the low-risk group. The overall levels of the immune score were higher in the high-risk group. Additionally, drug sensitivity analysis observed that the model could effectively predict efficacy and sensitivity to chemotherapy. Enrichment analysis revealed that the IL6-JAK-STAT3 signaling pathway was a major pathway. IL4I1 could promote ccRCC cells' proliferation, migration and invasion through JAK1/STAT3 signaling pathway and M2-like macrophage polarization.

**Conclusion:** The study elucidates that targeting fatty acids metabolism can affect the therapeutic effect of PD-1/PD-L1 in tumor immune microenvironment as well as related signal pathways. The model can effectively predict the response to several treatment options, underscoring its potential clinical utility.


# Introduction

Renal cell carcinoma (RCC) is the most common subtype of primary kidney cancer and results in numerous cases and deaths worldwide[1]. Immunocheckpoint therapies (ICTs) are the most rapidly growing clinical strategy for treating RCC and provide durable clinical benefits for patients with advanced ccRCC[2]. Simultaneously, two potential immune targets PD-1/PD-L1 as prognostic markers present in ccRCC. Antibodies against PD-1, including nivolumab and pembrolizumab, serve as a useful treatment of metastatic RCC [3, 4]. Nonetheless, unlike other immunotherapy-responsive solid tumors, many RCC patients show primary or adaptive resistance and adverse events to ICTs and not all patients show

complete responses[5], suggesting a further understanding of PD-1/PD-L1 mediated immunosuppression in RCC is needed to enhance treatment efficacy.

Tumor growth depends on oncogene-driven reprogramming of cell metabolism, which enables cancer cells to absorb nutrients, build macromolecules, and proliferate[6]. Increasing evidence shows that highly proliferative cancer cells have been found to increase the number of enzymes that are involved in lipid and cholesterol biosynthesis[7]. Lipid droplets stored by excess lipids and cholesterol and their quantity is related to tumor invasiveness [8, 9] . The increase of fatty acids in tumor microenvironment could cause the accumulation of lipid droplets and reprogramming lipid metabolism could impact indirectly on the function of immune cells and enhance tumor immunotherapy [10]. ccRCC is prominently featured with the accumulation of robust lipid as well as glycogen and associated with metabolic reprogramming for adaptation to the TME [11, 12], and different enzymes in fatty acids metabolism are potential biomarkers for diagnosis and promise for clinical effect in patients with ccRCC[13]. Due to the existence of a highly dynamic tumor microenvironment, and due to the glucose and fatty acids metabolism in ccRCC, this cancer could be accompanied by diverse types of resistance to ICIs. The intricate relationship between the abnormal fatty acids metabolism and the immune microenvironment in ccRCC has not yet been well illustrated. Therefore, the exploration of underlying relationships is crucial for future success in designing combination treatments to improve ccRCC patients' resistance to ICTs.

In the current study, we established novel fatty-acids-metabolism-related mRNA signatures based on the TCGA cohort to contribute to the prediction about ccRCC patients' survival prognosis. Additionally, the role of the target genes of these mRNAs in related immunotherapy of ccRCC was also clarified. The bioinformatics insights from this study will be valuable for future therapeutic development in ccRCC.

# Materials and Methods

### Data acquisition.

TCGA-KIRC datasets and clinical data of ccRCC (n = 526) and normal (n = 72) samples were retrieved from TGCA and were processed for subsequent analyses. The E-MTAB-1980 cohort was available on the ArrayExpress website (https://www.ebi.ac.uk/arrayexpress/). Normalized transcriptome and clinical matrix files of ccRCC patients treated with Nivolumab in the CheckMate-025 (CM-025) cohort were collected from published articles [14]. Other normalized gene expression profiles and clinic datasets of ccRCC patients from a randomized phase II trial (IMmotion150[15]) and a randomized phase III trial (IMmotion151[16]) were selected for analysis.

309 genes of fatty acids metabolism were acquired and collected from fatty acids metabolic pathways in KEGG, fatty acids metabolic genes in Hallmark and the specific genes associated fatty acids metabolism[17]. These fatty acids metabolism-related genes are provided in Table S1.

### Differential expression genes identification

309 genes expression between ccRCC and normal samples in TCGA-KIRC cohort was assessed with the “limma” R package. To further visualize differentially expressed fatty acids metabolism-related genes, the heatmap as well as volcano map were drawn. The thresholds of DEG were as follows: the fold change (FC) of differential expression of mRNAs was |log2 Fold Change| ≥ 1 and False Discovery Rate (FDR) < 0.05.

### Signature construction

Totally 526 ccRCC patients in TCGA-KIRC dataset included in the analysis were randomly divided into the train set (n = 395) and the test set (n = 131) by 3:1 ratio. Based upon the train set, the fatty acids metabolism-related DEGs were further analyzed through univariate Cox proportional hazard regression and simultaneously the least absolute shrinkage and selection operator (Lasso) analysis (through the "glmnet" R package[18]) to avoid overfitting. Multivariate cox proportional hazard regression analysis was applied to construct the prognosis model. The risk scores of each of the patients were established with the score determined as: Risk score = $\sum$ (expression of signature genes * corresponding coefficient). According to the median risk score, patients from datasets were assigned to high-risk or low-risk groups.

### Prognostic signature validation

Datasets including internal and external test sets were subsequently evaluated and used for calculating risk scores. The predictive capability of the signature was verified using ROC curves as well as KM survival curves (R packages “survival” and “survminer”). The individuals in the testing sets were allocated to groups by the same method as the training set. Furthermore, we also explored the predictive accuracy of nomograms through time-dependent ROC curves.

### Drug sensitivity analysis

To estimate the drug sensitivity in different risk groups, we performed drug sensitivity analysis utilizing the R package ("ggpubr") and calculated the IC50 through the R package ("pRRophetic")[19]. We therefore calculated the risk score of ccRCC cell lines through CCLE and drug sensitivity data in GDSC. Pearson correlation analysis was applied to identify the relationship between the risk score in ccRCC cell lines and the drug IC50 value.

### Immunotherapeutic effect analysis

Response to anti-PD-1/PD-L1 therapy in ccRCC patients was examined on three Immune-related cohorts (CheckMate-025, IMmotion150 and IMmotion151). The comparson was different risk scores in the stable disease/partial disease (SD/PD) as well as complete response/partial response (CR/PR) groups (R packages “ggsignif”, “ggplot2” and “ggpubr”). To predict the immunotherapeutic effect in different risk groups, the tumor immune dysfunction and exclusion (TIDE) (http://tide.dfci.harvard.edu/) was conducted and visualized through a violin plot.

### Enrichment analysis

Gene Ontology (GO) enrichment as well as Kyoto Encyclopedia of Genes and Genomes (KEGG) pathway analysis (R packages “clusterprofiler”) were utilized in this study and were further visualized by R package “ggplot2”. Gene set enrichment analysis (GSEA) was applied in this study and the “GSVA” R package was utilized to explore remarkably correlated pathways. Two annotated gene set file (“c2.cp.kegg.v7.4.symbols.gmt” as well as “c5.go.v7.5.1.symbols.gmt”) from the MSigDB database (https://www.gsea-msigdb.org/gsea/msigdb/) were chosen as the reference.

## Immunohistochemistry (IHC)

Paraffin sections of ccRCC tissues and normal tissues were deparaffinized and hydrated. Then, we performed antigen retrieval through microwave with citrate buffer (pH 9.0). To avoid the endogenous peroxidase activity, the sections were incubated in the slides in 0.3% $H_2O_2$ for 10min. Then, sections were manipulated with primary antibody at 4 °C for 12h and subsequently incubated with secondary antibody at room temperature for 1 h. After performing by peroxidase and 3,3-Diaminobenzidinetetrahydrochloride (DAB), sections were developed with hematoxylin and subsequently mounted in nonaqueous mounting medium. Images were captured with KF-PRO-020 Digital Slice Scanner. Two qualified pathologists evaluated and scored pathological samples separately. The anti-IL4I1 antibody (1:200, Abcam, ab176588) and anti-CD206 (1:1000, Proteintech, China) were respectively utilized to detect expression levels of IL4I1 and CD206 in different tissues.

## Cell culture and siRNA interference assay

Human renal proximal tubular epithelial cell line (HK2) and Human RCC cell lines (786-O, 769-P, ACHN, A498, CAKI-1, CAKI-2 and OSRC2) sprang from the American Type Culture Collection (ATCC). All cells were maintained in appropriate medium with 10% FBS and incubated with 5% $CO_2$ at 37°C. One scrambled siRNA (negative control) and three IL4I1 siRNAs were synthesized by (RiboBio, China) (Table S2). 786-O or 769-P was transfected with siRNAs through jetPRIME (Polyplus, French) on the basis of the manufacturer’s instructions. At 48 h after transfection, Functional assays were performed and protein and RNA were harvested.

## RNA expression

We extracted total RNAs from ccRCC cell lines and si-IL4I1-transfected 786-O or 769-P, as well as the ccRCC and adjacent normal samples of 10 KIRC patients using EZ-press RNA Purification Kit (EZBioscience, USA) and PrimeScript RT reagent kit (EZBioscience, China). The level of the mRNA IL4I1 was further examined through qRT-PCR with SYBR Green PCR reagent (EZBioscience, China) on Applied Biosystems™ QuantStudio™ 5 Real-Time PCR System in triplicate. Each mRNA expression was calculated with the 2-ΔΔCt method. All specific primers used in quantitative real-time PCR (qRT-PCR) are shown in Table S3. Human participants in these studies were reviewed and approved by the Institutional Ethics Committee for Clinical Research and Animal Trials of the First Affiliated Hospital of Sun Yat-sen University [(2021)144] and conformed to the standards set by the Declaration of Helsinki.

### Wound healing, cell migration and invasion assays

Cells were scratched with a pipette after cellular fusion into a six-well plate. Photos were taken at 0h and 24h after scratching. To evaluate the invasion and migration capability, 786O or 769P were starved in serum-free RPMI 1640 medium for 8 h. Then, $5\times10^4$ in 100 μl 786O or 769P in serum-free RPMI 1640 medium was added to transwell inserts (Corning, USA). The lower chamber of transwell assays was supplemented by serum-free RPMI 1640 medium with 10% FBS as a nutritional attractant. Lower surface cells after 8 h for migration assay and 16 h for invasion assay were respectively fixed with 4% polyformaldehyde (Beyotime, China) for 30 min, and stained with 0.4% crystalviolet (Beyotime, China) for 30 min. Invaded/migrated cells on the upper surface were wiped out with a cotton swab and those on the lower surface were counted under the microscope.

### Colony formation test

At 24 h after transfection, we inoculated 1000 786-O or 769-P cells into each well of the six-well plates, which were cultured for 2 weeks, then the colony was counted and analyzed.

### Coculture assay

THP-1 monocytes were induced and differentiated into M0 macrophages by PMA (Phorbol 12-myristate 13-acetate). Once differentiated (M0 macrophages), they were incubated respectively with cell supernatant of ccRCC cell line (786O or 769P) transfected with IL4I1 siRNA for 48 hours. The impact of the knock-down of IL4I1 on macrophage polarization was assessed by western blot for CD206 protein and flow cytometry of the proportion of M2 macrophage.

### Flow cytometry

Expression of M2 macrophage maker CD206 was examined through flow cytometry. The cells were detached with trypsin, washed and blocked with PBS + 1%BSA solution, and then incubated with CD206 (321104, Biolegend, California, USA). The cells were then analyzed by a Beckman CytoFlex LX instrument and analyzed by FlowJo software.

### Western blot

RIPA lysis buffer (ThermoFisher, USA) containing protease and phosphatase inhibitors (MCE) was utilized to extract total proteins incubated on ice for 15 min. Then, after centrifuged for 2 min (12,000 g, 4 °C) and supernatants collected, protein concentration was measured with a BCA protein assay kit (ThermoFisher, USA). After denaturation with 5x SDS-PAGE gels, the proteins were electrophoresed in 12% SDS-polyacrylamide gels (Bio-Rad) and transferred onto 0.2um PVDF membranes (Millipore) blocked in skim milk for 1h. Then, membranes were incubated for 12h with the primary antibody at 4 °C, and subsequently with the secondary antibody at room temperature for 1 h. Antibodies for western blots were as follows: IL4I1 (1:200, Abcam, ab176588), CD206 (1:1000, Proteintech, China).

### Statistical Analysis

Pearson or Spearman coefficients were used to analyze correlations between variables. R language v4.0.2 (https://www.r-project.org/) and GraphPad Prism 8.0 software were conducted for data analysis. The evaluation of the difference between two groups was analyzed with the Wilcoxon rank-sum test. The significance of the two group differences was $P<0.05$.

# Results

### Construction of the prognostic model

A total of 309 genes related with fatty acids metabolism were included in this study. After TCGA datasets filtering, quality assessment and data processing, 96 DEGs were finally extracted through the “limma” R package and the results indicated that 62 DEGs were downregulated and 34 DEGs were upregulated. The heatmap and volcano map was used to visualize DEGs **(Figures 1b, 1c)**. The prognostic model was developed based on univariate and multivariate Cox regression analysis as well as LASSO analysis **(Figures 1d, 1e)**. Ultimately, the prognostic model was visualized by “forest” **(Figure 1f)** consisting of 20 genes: HACD1, HPGD, ALOX15B, ABCD1, HMGCS2, CPT1B, TDO2, SCD5, PCCA, DPEP1, ALAD, ACADM, ACADSB, ACAT1, PLA2G4A, ALOX12B, IL4I1, ACAD11, HIBCH, LTC4S. Risk score= (0.319240 * HACD1) + (-0.084391 * HPGD) + (-0.180228 * ALOX15B) + (0.459381 * ABCD1) + (-0.063391 * HMGCS2) + (0.325758 * CPT1B) + (0.140669 * TDO2) + (-0.029671 * SCD5) +(0.127550 * PCCA) + (-0.067707 * DPEP1) + (-0.342020 * ALAD) + (-0.040588 * ACADM) + (0.131207 * ACADSB) + (-0.110134 * ACAT1) + (-0.161595 * PLA2G4A) + (-0.407284 * ALOX12B) + (0.280250 * IL4I1) + (-0.028668 * ACAD11) + (-0.158444 * HIBCH) + (-0.766512 * LTC4S).

### Prognostic model validation

The ROC curves and the KM curves were utilized to explore the predictive power of the prognostic model on the internal and external test sets. The area under the ROC curve (AUC) of the 3-, 5-, and 7-year in TCGA-KIRC train and test cohort as well as E-MTAB-1980 cohort presented good prediction performance **(Figures 2a-2c)**. Using the same prognostic model, we classified the remaining patients in all the test sets into different risk groups based on the median of all risk scores. The risk score of the prognostic model in TCGA-KIRC train and test as well as E-MTAB-1980 cohort was an independent protective factor of overall survival (OS). Patients with high-risk scores exhibited significantly lower OS compared to those in the low-risk group **($P<0.05$, Figures 2d, 2e)**. K-M analysis further revealed that ccRCC patients with high-risk score had lower progression-free-survival (PFS) in TCGA-KIRC cohort **($P<0.05$, Figures S1a-S1d)**.

### The clinicopathological characteristics in TCGA-KIRC cohort

As shown in **Figure 3a**, a clinical correlation analysis was performed, demonstrating that grade and stage levels increased with the risk score of the prognostic model **($P<0.05$, Figure 3a)**. Moreover, the risk score exhibited superior predictive power, with the largest area under the ROC curve compared to age, gender,

grade, and stage **(Figure 3b)**. Furthermore, the AUC values of the 3-, 5-, and 7-year in TCGA-KIRC total cohort were 0.745, 0.765, and 0.742 respectively **(Figure 3c)**. Subsequently, based on the clinical features and risk score, a nomogram for OS prediction was conducted and composed of age, stage as well as risk score as the independent prognostic factors (*P* 0.05) (see Figure 3d). In the calibration diagram **(Figure 3e)**, the 1-, 3-, and 5-year OS for ccRCC individuals had a good predictive performance of this personalized nomogram model (C-index = 0.779).

### The immune landscape of the prognostic model and response to anti-PD-1/ PD-L1 therapy

The response to anti-PD-1/ PD-L1 therapy was examined based on the immune-related cohorts (CheckMate-025, IMmotion150 and IMmotion151), and results indicated that different risk groups between SD/PD and CR/PR possessed a statistically significant difference. Not surprisingly, results from the immune-related databases revealed that the high-risk group processes a significantly lower response to anti-PD-1/ PD-L1 therapy **(Figure 3f)**. Further, through the TIDE algorithm, high-risk group in the TCGA-KIRC database had a high potential of immune escape with a worse effect of immunotherapy **(Figure 3g)**. Applying the ESTIMATE algorithm, we calculated the overall levels of the immune score. The immune score of the high-risk group was higher than low-risk group **(Figures 3h)**.Moreover, as expected, in IMmotion150 and IMmotion151 cohorts, the low-risk group for survival was linked to higher PFS **(*P*0.05, Figure 3i)**. We then performed a hierarchically K-M analysis of the CheckMate-025 study. The results indicated there was a significant difference in the survival rate between different risk groups in the ccRCC patients with Nivolumab monotherapy from the CheckMate-025 cohort while there was no significant difference in those treated with Everolimus (a mammalian target of mTOR inhibitor) **(Figures S1d,1e)**, suggesting that our model is more effective and suitable for anti-PD-1/ PD-L1 therapy in the ccRCC patients. Subsequently, in the comparison of several immune signatures, inflammation-promoting, T cell co-stimulation, checkpoint, antigen-presenting cell (APC) co-stimulation, chemokine receptors (CCR), and Type I IFN response were found to be higher in the high-risk group than the low-risk group, while type II IFN response was obviously downregulated (see Figure 3j). Additionally, TME cell composition and fraction of individual immune cell types in three Immune-related cohorts were computed and generated with CIBERSORT (http://cibersort.stanford.edu/). We observed that the high-risk groups presented a higher fraction of M0 macrophages than the low-risk group **(*P*0.05, see Figures S2a-2c)**, thus highlighting the risk score of our model could predict clinical response to ICI-based immunotherapy.

### Risk scores and drug sensitivity analysis

We conducted drug sensitivity analysis based on the different risk groups through the “pRRophetic” package and the IC50 value was utilized to measure the sensitivity to drugs **(Figure 4a)**. The high-risk group possessed significantly higher IC50 values but was less sensitive to the drugs than the group with low-risk (*P* 0.05). For quantifying the individual patients, the correlations between risk score of prognostic model and targeted drugs was assessed through the “ggplot” package and identified that Sorafenib, Erlotinib, Saracatinib and Crizotinib had high degree of correlation with risk score of prognostic model, suggesting that the constructed model could effectively predict efficacy and sensitivity to

chemotherapy **(Figures 4b)**. We further evaluated the risk score of ccRCC cell lines through CCLE and drug sensitivity data from GDSC. The results indicated that A498 had the highest risk score while BFTC-909 had the lowest risk score, which implied that higher malignancy existed in A498 compared with other cell lines **(Figure S3a)**. Pearson correlation analysis suggested that the risk score had a positive correlation with IC50 of C-75 (an inhibitor of fatty acids synthase), while was negatively correlated with IC50 of PD0325901 (an oral potent ERK inhibitor) **(Figure S3b)**. These revealed that the higher risk score was more sensitive to PD0325901 and less to C-75, which might be an effective targeted therapy of ccRCC.

### Identifying related pathways and immune checkpoints

We utilized ssGSEA to examine the correlations between the risk score and the enrichment scores of related pathways or immune checkpoints to explore the immune-related functional processes. Our findings revealed a positive correlation between the risk score and JAK-STAT3 signaling, as well as major immune checkpoints **(Figures 4c, 4d)**. These implied that fatty acids metabolism in ccRCC was associated with JAK-STAT3 signaling and the risk score levels could reflect the therapeutic effect of ccRCC patients treated with anti-PD-1/ PD-L1.

### Enrichment analysis and GSEA hallmark visualization

To confirm the underlying mechanism of JAK-STAT3 signaling and fatty acids metabolism in ccRCC progression, we performed GSEA on TCGA-KIRC cohort. The results based on GSEA analysis indicated that differentially expressed target genes are enriched in immune and metabolism-related functional pathways. The upregulated DEGs groups, in particular, were enriched in JAK-STAT3 signaling. Meanwhile, fatty acids metabolism was observed in the downregulated DEGs groups (see Figure 4e). KEGG enrichment analysis was developed for tumorigenic pathways enrichment analysis in TCGA-KIRC cohort which demonstrated an association with cytokine-cytokine receptor interaction, fatty acids metabolism and complement and coagulation cascades **(Figure 4f)**. GO analysis was performed to further explore the potential biological processes of DEGs and revealed that most immune responses and associated activities were significantly enriched in these genes **(Figure 4g)**. Thus, these results indicated that the fatty acids metabolism might contribute to ccRCC development mainly concentrated on immune response.

### Evaluation of joint indicators and multi model comparison

To establish the superiority of our model, we conducted a comparison of the accuracy of several immune indicators and previous studies in the TCGA-KIRC cohort. [20]. The ROC curve indicated that the AUC of the risk score is significantly higher than other indicators and other fatty acids metabolism-related model, suggesting that our model was more accurate**(Figure 4h)**. Overall, the constructed model demonstrated greater representativeness in fatty acids metabolism compared to other network models or indicators.**Validation of mRNA expression**

To analyze the mRNA expression profiles, we explored the expression levels of 6 fatty acids metabolism-related genes in our risk model in tumor and normal tissues as well as ccRCC cell lines. The qPCR results indicated that the expression levels of ABCD1, ALOX12B, ALOX15B, HACD1, IL4I1 significantly upregulated in tumor samples, while the expression of CPT1B was low in RCC tissues **(Figures 5a, 5b)**. Similarly, the expression patterns of these six genes were also observed in ccRCC cell lines **(Figure 5c)**. Additionally, oligo sequences in the qPCR were displayed in Supplementary Table S2.

### Silencing IL4I1 suppresses the growth and invasion of ccRCC cells

To elucidate the role of IL4I1 in ccRCC migration and invasion in vitro, three siRNA specifically targeting IL4I1 (si-IL4I1-1, si-IL4I1-2 and si-IL4I1-3) were constructed respectively **(Figure 5d)**. Transwell assays revealed that the migration and invasion capabilities of 786-O and 769-P were inhibited after the silence of IL4I1 **(Figure 6a)**. Furthermore, in accordance with the above results, colony formation assays and wound healing demonstrated that silencing IL4I1 significantly suppresses the proliferation of 786-O and 769-P **(Figures 6b, 6c)**. Altogether these results collectively elucidated that IL4I1 could promote the growth and invasion of ccRCC cells.

### Silencing IL4I1 impacts JAK1/STAT3 signaling pathway

Based on the above analysis about our model, GSEA suggested that our model strongly associated with JAK1/STAT3 signaling pathway **(Figure 5e)**. To further clarify the effects of IL4I1 on JAK1/STAT3 signaling pathway, western blot was assessed to test IL4I1's contribution to the functional outcomes of JAK1/STAT3 signaling pathway. The result showed that silencing IL4I1 downgrades the expression of phosphorylated JAK1 and phosphorylated STAT3 **(Figure 5f)**, suggesting that IL4I1 could modulate JAK1/STAT3 signaling pathway and lead to JAK1/STAT3 phosphorylation.

### Silencing IL4I1 inhibits M2-like macrophages polarization

To investigate whether IL4I1 signaling to Chemokine ligand 2 (CCL2) could mediate macrophages polarization, an indirect co-culture condition between si-IL4I1-transfected 786-O and 769-P as well as M0-like macrophages was conducted. Flow cytometry results revealed that silencing IL4I1 inhibited M2-like macrophages polarization **(Figures 7b,7c)**. Additionally, western blot also implied that silencing IL4I1 could suppress the level of CD206 (M2 macrophage surface marker) (see Figure 7d) and even CCL2 expression of si-IL4I1-transfected ccRCC cells (786-O and 769-P) **(Figure 5f).** Moreover, IHC staining validated that the high expression of IL4I1 and CD206 in tumor samples were simultaneously higher than that in adjacent normal tissues **(Figure 7a)**. In summary, these results proved that the knockdown of IL4I1 in si-IL4I1-transfected 786-O and 769-P inhibited M2-like macrophage polarization engaged by the regulation of CCL2.

# Discussion

The dynamic fatty acids metabolism disorder of malignant cells has a profound influence on tumor-targeting immune responses in TME. Dysregulated fatty acids metabolism can lead to the accumulation of lipids, which in turn can modulate the activity of tumor-associated macrophages (TAMs) and suppress immune surveillance [12] [21]. In particular, high expression of fatty acids synthase (FAS) serves as an adverse predictive marker for survival prognosis[22].. Correspondingly, the JAK/STAT signaling pathway is essential in M1 and M2 macrophage polarization[23], with upregulated fatty acids oxidation enhancing phosphorylation of JAK1 as well as STAT6 activation to regulate the generation of M2-like TAM[24]. While a previous report has constructed a prognosis model for fatty acids metabolism in ccRCC[20], it lacks satisfactory predictive abilities, and is unable to associate tumor immune microenvironment with fatty acids metabolism through a well-defined method, lacking the corresponding immune validation set and experimental evidence.

In the study, we constructed a fatty acids metabolism-related prognosis model and explored mechanisms that fatty acids metabolism impacts on the therapeutic effect of anti-PD-1/PD-L1 in tumor immune microenvironment in ccRCC. Based on related fatty-acids-metabolism-related genes in TCGA-KIRC train cohort, an efficient prognostic model for ccRCC patients consisting of 20 genes was constructed through univariate and multivariate Cox regression analysis as well as LASSO analysis. We further explore the prognostic value of model on the internal and external test sets through ROC curves and KM curves by the median of all risk scores. The AUC of the TCGA-KIRC train, and test cohort as well as E-MTAB-1980 cohort demonstrated a good prognostic efficiency. Additionally, ccRCC patients with high-risk score in all cohorts had significantly lower survival probability. High-risk groups were found to be correlated with higher tumor grade and advanced pathologic stage in the TCGA-KIRC cohort.. Subsequently, a new nomogram was conducted including independent prognostic factors (age, stage, and risk score) and had a good predictive performance. For the purpose of promotion in immunotherapy in ccRCC patients, based on three Immune-related cohorts (CheckMate-025, IMmotion150 and IMmotion151), results indicated that high-risk group had a significantly lower response to anti-PD-1/ PD-L1 therapy. Further investigation revealed that a high potential of immune escape phenotype existed in the high-risk group in the TCGA-KIRC cohort through the TIDE algorithm, implying that high risk score in this model predicts poor prognosis in ccRCC patients treated with immunotherapy. In addition, we also found that the higher immune score occurred in the high-risk group. Therefore, our findings provide a model to identify which type of ccRCC patients are more suitable for immunotherapy and achieve a better curative effect. ccRCC is more frequently known as a proinflammatory neoplasia and can recruit polyclonal $CD8^+$T cells through cytokines production[25-28]. However, high densities of $CD8^+$T cells are involved in the poor clinical prognosis of ccRCC patients[29]. Consistent with these findings, immune signatures analysis in TCGA-KIRC cohort suggested that inflammation-promoting, T cell co-stimulation, checkpoint, CCR, and Type I IFN response were found to be higher in the high-risk group than the low-risk group. Our findings also observed that the high-risk group presented significantly higher IC50 values and was less sensitive to the agents than the low-risk group. To aid in clinical decision-making, drug sensitivity, Pearson correlation analysis were performed and indicated that the risk score had positive correlation with IC50 of C-75. Interestingly, C75 is an inhibitor of fatty acids synthase (FAS) which triggers apoptosis during S phase

and inhibits fatty acids synthesis in liver cancer[30, 31], which might be an effective targeted therapy of ccRCC. To analyze if the model could provide new indications for immunotherapy, it was noteworthy that the related functional pathways or immune checkpoints were recognized to be positively correlated with IL6-JAK-STAT3 signaling and prominent immune checkpoints (including PD-1, PD-L1, LAG-3, and CTLA4). We compared the accuracy of several associated immune indicators and previous studies in the TCGA-KIRC cohort and found that the risk score had a significantly higher area under the ROC curve (AUC) than other indicators and previous models related to fatty acids metabolism. Additionally, we performed RT-qPCR to consistently evaluated the expression levels of ABCD1, ALOX12B, ALOX15B, HACD1, IL4I1, CPT1B by RT-qPCR. Among the 20 genes, ATP-binding-cassette transporter subfamily D member 1 (ABCD1) was shown to transport very long chain fatty acyl-CoAs from cytosol to peroxisome for β-oxidation[32], and mutations of the ABCD1 might cause X-linked adrenoleukodystrophy[33]. Arachidonate 12-lipoxygenase, 12R type (ALOX12B) can convert arachidonic acids to 12R-hydroxyeicosatetraenoic acids 8 and is responsible for immune activity blocking the uptake of apoptotic cells through inflammatory monocytes which reduces antigen presentation to T cells in tumor[34]. Arachidonate 15-lipoxygenase, type B (ALOX15B) upregulated in RCC-infiltrating macrophages, mediates lipid metabolism in TAMs and contributes to tumor progression as well as tumor immunity[35, 36]. 3-hydroxyacyl-CoA dehydratase 1 (HACD1) has been implicated as a regulator in the membrane composition and fluidity and elongate the very long chain fatty acids[37]. Carnitine palmitoyltransferase 1B (CPT1B) exerts rate-controlling-enzyme roles in fatty acids β-oxidation, could be inhibited by Inhibiting JAK/STAT3 promoting breast cancer cells to re-sensitize to chemotherapy [38]. More importantly, Interleukin-4-induced-1 (IL4I1) as a metabolic immune checkpoint, activates the Aryl hydrocarbon receptor (AHR), circumvents Immune Checkpoint Blockade (ICB) and further elicits major effects in immunosuppression shaping tumor microenvironment [39]. In addition, the expression of IL4I1 by tumor cells related to immune regulatory mechanisms determines T-lymphocyte inhibition in the tumor microenvironment. IL4I1 is involved in different infiltrating lymphocytes to enhance tumor malignancy [40]. The above observations highlighted that IL4I1 processes promote effects on tumor occurrence, and pleaded for scrutiny in the role of IL4I1 as a prognosis factor in the crosstalk of fatty acids metabolic reprogramming and immune regulatory functions in ccRCC. Simultaneously, considering that IL4I1 as a prognosis predictive gene engages in our constructed model, we scrutinized the role of IL4I1 involved in tumor immune escape in ccRCC. Here, we noted that the proliferation, migration and invasion capability of ccRCC cells silencing IL4I1 were decreased. Beyond its correlations with immune processes, the results based on GSEA analysis revealed that IL4I1 was enriched in the following activated pathways, containing IL6-JAK-STAT3 signaling. GO functional enrichment analysis exhibited that most immune responses and associated activities were mainly enriched in these genes. KEGG indicated its association with fatty acids metabolism. In addition, arachidonic acids alters lipid raft structures to inhibit JAK1and STAT3 phosphorylation in the ovarian cancer microenvironment where high CD206 expression is in TAMs[41].To further clarify the effects of IL4I1 on JAK1/STAT3 signaling pathway, western blot was assessed to test IL4I1's contributions to the functional outcomes of JAK1/STAT3 signaling pathway. Together, these findings implied that IL4I1 could modulate JAK1/STAT3 signaling pathway and lead to JAK1/STAT3 phosphorylation. Metabolism regulates macrophage polarization through cytokines and other signaling mediators modulating the

immune response in TME [42]. Additionally, CCL2 is a chemokine that is secreted by tumor cells to recruit and activate immune cells and further facilitate anti-tumor activities in TME [43]. To explore if IL4I1 signaling to CCL2 could mediate macrophages polarization, an indirect co-culture condition between si-IL4I1-transfected ccRCC cells (786-O and 769-P) and M0-like macrophages was conducted and revealed that silencing IL4I1 inhibited M2-like macrophages polarization associated with JAK1/STAT3 phosphorylation and CCL2 expression.

To summarize, we describe a novel mechanism underlying fatty acids metabolism that promotes the crosstalk within and across cancer cells and immune cells in ccRCC tumor microenvironment. However, several limitations still exist.  Firstly, the optimal cut-off value of risk score was not determined and the median risk score was used as a surrogate. Furthermore, additional in vivo and in vitro experiments are required to further elucidate the comprehensive role of the fatty acids metabolism-related prognostic model in ccRCC.. However, this study represents the most systematical and comprehensive investigation that elucidates how the fatty acids metabolism influences resistance to immunotherapy in ccRCC, which could serve as potentially a potent orientation to evaluate low immune responses in ccRCC patients.

# Conclusion

This study demonstrated that fatty acids metabolism affects alternative polarization of immune cells correlated with JAK1/STAT3 signaling pathway and CCL2, further influencing the therapeutic effect of PD-1/PD-L1 to ccRCC in tumor immune microenvironment.

# Abbreviations

RCC: Renal cell carcinoma

ccRCC: Clear Cell Renal Cell Carcinoma

ICTs: Immunocheckpoint therapies

TME: Tumor microenvironment

PD-1: Programmed death-1 receptor

PD-L1: Programmed death-1 receptor-ligand

TIDE: Tumor immune dysfunction and exclusion

FC: Fold change

FDR: False Discovery Rate

Lasso: Least absolute shrinkage and selection operator

SD/PD: Disease/partial disease

CR/PR: Complete response/partial response

GSEA: Gene set enrichment analysis

ssGSEA: Single sample Gene set enrichment analysis

GSVA: Gene set variation analysis

KEGG: Kyoto encyclopedia of genes and genomes

KIRC: Kidney renal clear cell carcinoma

TCGA: The Cancer Genome Atlas

FAS: Fatty acids synthase

CCL2: Chemokine ligand 2

TAM: Tumor-associated macrophages

CCLE: Cancer Cell Line Encyclopedia

GDSC: Genomics of Drug Sensitivity in Cancer

AHR: Aryl hydrocarbon receptor

ICB: Immune Checkpoint Blockade

OS: Overall survival

PFS: Progression free survival

DAB: 3,3-Diaminobenzidinetetrahydrochloride

IL4I1: Interleukin-4-induced-1

CPT1B: Carnitine palmitoyltransferase 1B

ABCD1: ATP-binding-cassette transporter subfamily D member 1

ALOX12B: Arachidonate 12-lipoxygenase, 12R type

ALOX15B: Arachidonate 15-lipoxygenase, type B

HACD1: 3-hydroxyacyl-CoA dehydratase 1

HPGD: 15-hydroxyprostaglandin dehydrogenase

HMGCS2: 3-hydroxy-3-methylglutaryl-CoA synthase 2

TDO2: Tryptophan 2,3-dioxygenase

SCD5: Stearoyl-CoA desaturase 5

PCCA: Propionyl-CoA carboxylase subunit alpha

DPEP1: Dipeptidase 1

ALAD: Aminolevulinate dehydratase

ACADM: acyl-CoA dehydrogenase medium chain

ACADSB: acyl-CoA dehydrogenase short/branched chain

ACAT1: acetyl-CoA acetyltransferase 1

PLA2G4A: Phospholipase A2 group IVA

ACAD11: acyl-CoA dehydrogenase family member 11

HIBCH: 3-hydroxyisobutyryl-CoA hydrolase

LTC4S: leukotriene C4 synthase

JAK/STAT3: Janus tyrosine kinase1/ Signal transducer and activator of Transcription3

# Declarations


### Acknowledgements

Not applicable.

### Funding

This research was partially or fully sponsored by The National Natural Science Foundation of China (No.81902576, No.82272862, No.82002684, No.82103587) and Guangzhou Science and Technology Projects (202201010910).


### Availability of data and materials

Any reasonable requests for access to available data underlying the results reported in this article will be considered. Such proposals should be submitted to the corresponding author.

### Authors' contributions

HSL, LMF and PJL designed the study. JQZ, QHX, MAM, YHW, XWZ and YHC obtained and assembled data. GSY, JYL, JHB and YQZ conducted the vitro experiments. JL and LZZ analyzed and interpreted the data. JZC wrote the manuscript, which was edited by all authors, who have approved the final version for submission. HSL, LMF, PJL and JQZ contributed equally to this paper. All authors read and approved the final manuscript.

### Ethics approval and consent to participate

This study was approved by the Ethics Committee of the First Affiliated Hospital, Sun Yat-sen University. Informed consent was waived because data were deidentified.

### Consent for publication

Not applicable.

### Competing interests

The authors declare that they have no conflict of interest.

# References


1. Siegel, R.L., K.D. Miller, H.E. Fuchs, et al., *Cancer statistics, 2022.* CA Cancer J Clin, 2022. **72**(1): p. 7-33.
2. Barata, P.C. and B.I. Rini, *Treatment of renal cell carcinoma: Current status and future directions.* CA Cancer J Clin, 2017. **67**(6): p. 507-524.
3. Motzer, R.J., N.M. Tannir, D.F. McDermott, et al., *Nivolumab plus Ipilimumab versus Sunitinib in Advanced Renal-Cell Carcinoma.* N Engl J Med, 2018. **378**(14): p. 1277-1290.
4. Motzer, R., B. Alekseev, S.Y. Rha, et al., *Lenvatinib plus Pembrolizumab or Everolimus for Advanced Renal Cell Carcinoma.* N Engl J Med, 2021. **384**(14): p. 1289-1300.
5. Braun, D.A., Z. Bakouny, L. Hirsch, et al., *Beyond conventional immune-checkpoint inhibition - novel immunotherapies for renal cell carcinoma.* Nat Rev Clin Oncol, 2021. **18**(4): p. 199-214.
6. Pavlova, N.N. and C.B. Thompson, *The Emerging Hallmarks of Cancer Metabolism.* Cell Metab, 2016. **23**(1): p. 27-47.
7. Beloribi-Djefaflia, S., S. Vasseur, and F. Guillaumond, *Lipid metabolic reprogramming in cancer cells.* Oncogenesis, 2016. **5**: p. e189.
8. Qiu, B., D. Ackerman, D.J. Sanchez, et al., *HIF2alpha-Dependent Lipid Storage Promotes Endoplasmic Reticulum Homeostasis in Clear-Cell Renal Cell Carcinoma.* Cancer Discov, 2015. **5**(6): p. 652-67.
9. Accioly, M.T., P. Pacheco, C.M. Maya-Monteiro, et al., *Lipid bodies are reservoirs of cyclooxygenase-2 and sites of prostaglandin-E2 synthesis in colon cancer cells.* Cancer Res, 2008. **68**(6): p. 1732-40.

10. Butler, L.M., Y. Perone, J. Dehairs, et al., *Lipids and cancer: Emerging roles in pathogenesis, diagnosis and therapeutic intervention.* Adv Drug Deliv Rev, 2020. **159**: p. 245-293.
11. Braun, D.A., K. Street, K.P. Burke, et al., *Progressive immune dysfunction with advancing disease stage in renal cell carcinoma.* Cancer Cell, 2021. **39**(5): p. 632-648 e8.
12. Du, W., L. Zhang, A. Brett-Morris, et al., *HIF drives lipid deposition and cancer in ccRCC via repression of fatty acid metabolism.* Nat Commun, 2017. **8**(1): p. 1769.
13. Tan, S.K., H.Y. Hougen, J.R. Merchan, et al., *Fatty acid metabolism reprogramming in ccRCC: mechanisms and potential targets.* Nat Rev Urol, 2022.
14. Braun, D.A., Y. Hou, Z. Bakouny, et al., *Interplay of somatic alterations and immune infiltration modulates response to PD-1 blockade in advanced clear cell renal cell carcinoma.* Nat Med, 2020. **26**(6): p. 909-918.
15. Powles, T., D.F. McDermott, B. Rini, et al., *IMmotion150: Novel radiological endpoints and updated data from a randomized phase II trial investigating atezolizumab (atezo) with or without bevacizumab (bev) vs sunitinib (sun) in untreated metastatic renal cell carcinoma (mRCC).* Annals of Oncology, 2017. **28**.
16. Rini, B.I., T. Powles, M.B. Atkins, et al., *Atezolizumab plus bevacizumab versus sunitinib in patients with previously untreated metastatic renal cell carcinoma (IMmotion151): a multicentre, open-label, phase 3, randomised controlled trial.* The Lancet, 2019. **393**(10189): p. 2404-2415.
17. Currie, E., A. Schulze, R. Zechner, et al., *Cellular fatty acid metabolism and cancer.* Cell Metab, 2013. **18**(2): p. 153-61.
18. Engebretsen, S. and J. Bohlin, *Statistical predictions with glmnet.* Clin Epigenetics, 2019. **11**(1): p. 123.
19. Geeleher, P., N. Cox, and R.S. Huang, *pRRophetic: an R package for prediction of clinical chemotherapeutic response from tumor gene expression levels.* PLoS One, 2014. **9**(9): p. e107468.
20. Nie, S., Y. Huili, A. Yao, et al., *Identification of subtypes of clear cell renal cell carcinoma and construction of a prognostic model based on fatty acid metabolism genes.* Front Genet, 2022. **13**: p. 1013178.
21. Wu, H., Y. Han, Y. Rodriguez Sillke, et al., *Lipid droplet-dependent fatty acid metabolism controls the immune suppressive phenotype of tumor-associated macrophages.* EMBO Mol Med, 2019. **11**(11): p. e10698.
22. Kuhajda, F.P., *Fatty acid synthase and cancer: new application of an old pathway.* Cancer Res, 2006. **66**(12): p. 5977-80.
23. Lawrence, T. and G. Natoli, *Transcriptional regulation of macrophage polarization: enabling diversity with identity.* Nat Rev Immunol, 2011. **11**(11): p. 750-61.
24. Su, P., Q. Wang, E. Bi, et al., *Enhanced Lipid Accumulation and Metabolism Are Required for the Differentiation and Activation of Tumor-Associated Macrophages.* Cancer Res, 2020. **80**(7): p. 1438-1450.

25. Van den Hove, L.E., S.W. Van Gool, H. Van Poppel, et al., *Phenotype, cytokine production and cytolytic capacity of fresh (uncultured) tumour-infiltrating T lymphocytes in human renal cell carcinoma.* Clin Exp Immunol, 1997. **109**(3): p. 501-9.
26. Shabtai, M., H. Ye, Z. Frischer, et al., *Increased expression of activation markers in renal cell carcinoma infiltrating lymphocytes.* J Urol, 2002. **168**(5): p. 2216-9.
27. Sittig, S.P., T. Køllgaard, K. Grønbæk, et al., *Clonal expansion of renal cell carcinoma-infiltrating T lymphocytes.* Oncoimmunology, 2013. **2**(9): p. e26014.
28. Gerlinger, M., S.A. Quezada, K.S. Peggs, et al., *Ultra-deep T cell receptor sequencing reveals the complexity and intratumour heterogeneity of T cell clones in renal cell carcinomas.* J Pathol, 2013. **231**(4): p. 424-32.
29. Giraldo, N.A., E. Becht, F. Pagès, et al., *Orchestration and Prognostic Significance of Immune Checkpoints in the Microenvironment of Primary and Metastatic Renal Cell Cancer.* Clin Cancer Res, 2015. **21**(13): p. 3031-40.
30. Zhou, W., P.J. Simpson, J.M. McFadden, et al., *Fatty acid synthase inhibition triggers apoptosis during S phase in human cancer cells.* Cancer Res, 2003. **63**(21): p. 7330-7.
31. Kuhajda, F.P., E.S. Pizer, J.N. Li, et al., *Synthesis and antitumor activity of an inhibitor of fatty acid synthase.* Proc Natl Acad Sci U S A, 2000. **97**(7): p. 3450-4.
32. Lauer, A., X. Da, M.B. Hansen, et al., *ABCD1 dysfunction alters white matter microvascular perfusion.* Brain, 2017. **140**(12): p. 3139-3152.
33. O'Neill, G.N., M. Aoki, and R.H. Brown, Jr., *ABCD1 translation-initiator mutation demonstrates genotype-phenotype correlation for AMN.* Neurology, 2001. **57**(11): p. 1956-62.
34. Uderhardt, S., M. Herrmann, O.V. Oskolkova, et al., *12/15-lipoxygenase orchestrates the clearance of apoptotic cells and maintains immunologic tolerance.* Immunity, 2012. **36**(5): p. 834-46.
35. Reinartz, S., F. Finkernagel, T. Adhikary, et al., *A transcriptome-based global map of signaling pathways in the ovarian cancer microenvironment associated with clinical outcome.* Genome Biol, 2016. **17**(1): p. 108.
36. Weigert, A., E. Strack, R.G. Snodgrass, et al., *mPGES-1 and ALOX5/-15 in tumor-associated macrophages.* Cancer Metastasis Rev, 2018. **37**(2-3): p. 317-334.
37. Blondelle, J., Y. Ohno, V. Gache, et al., *HACD1, a regulator of membrane composition and fluidity, promotes myoblast fusion and skeletal muscle growth.* J Mol Cell Biol, 2015. **7**(5): p. 429-40.
38. Wang, T., J.F. Fahrmann, H. Lee, et al., *JAK/STAT3-Regulated Fatty Acid β-Oxidation Is Critical for Breast Cancer Stem Cell Self-Renewal and Chemoresistance.* Cell Metab, 2018. **27**(1): p. 136-150.e5.
39. Sadik, A., L.F. Somarribas Patterson, S. Ozturk, et al., *IL4I1 Is a Metabolic Immune Checkpoint that Activates the AHR and Promotes Tumor Progression.* Cell, 2020. **182**(5): p. 1252-1270 e34.
40. Carbonnelle-Puscian, A., C. Copie-Bergman, M. Baia, et al., *The novel immunosuppressive enzyme IL4I1 is expressed by neoplastic cells of several B-cell lymphomas and by tumor-associated macrophages.* Leukemia, 2009. **23**(5): p. 952-60.

41. Hammoud, M.K., R. Dietze, J. Pesek, et al., *Arachidonic acid, a clinically adverse mediator in the ovarian cancer microenvironment, impairs JAK-STAT signaling in macrophages by perturbing lipid raft structures.* Mol Oncol, 2022. **16**(17): p. 3146-3166.
42. Mehla, K. and P.K. Singh, *Metabolic Regulation of Macrophage Polarization in Cancer.* Trends Cancer, 2019. **5**(12): p. 822-834.
43. Li, X., W. Yao, Y. Yuan, et al., *Targeting of tumour-infiltrating macrophages via CCL2/CCR2 signalling as a therapeutic strategy against hepatocellular carcinoma.* Gut, 2017. **66**(1): p. 157-167.

# Figures

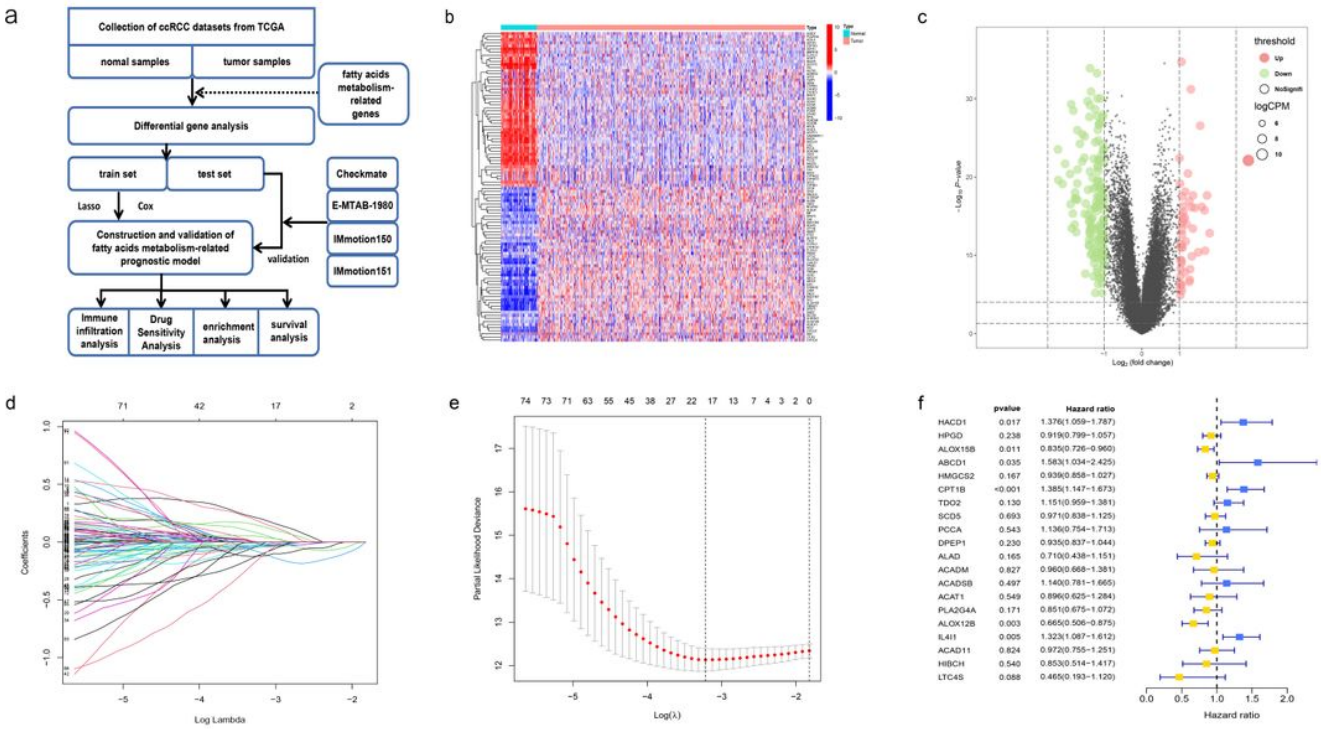


**Figure 1**

Overview of the study design and construction of the prognostic model. (a)Flow-chart of bioinformatics. (b) Heatmap of the differentially expressed fatty acids metabolism genes in KIRC. (c)Volcano plot of the downregulated and upregulated fatty acids metabolism-related DEGS. (d) Prognostic model construction by LASSO Cox analysis. (e)Cross-validation for the minimum lambda value in the LASSO regression model. (f) Forest plot of the prognostic model in multivariate cox analysis.

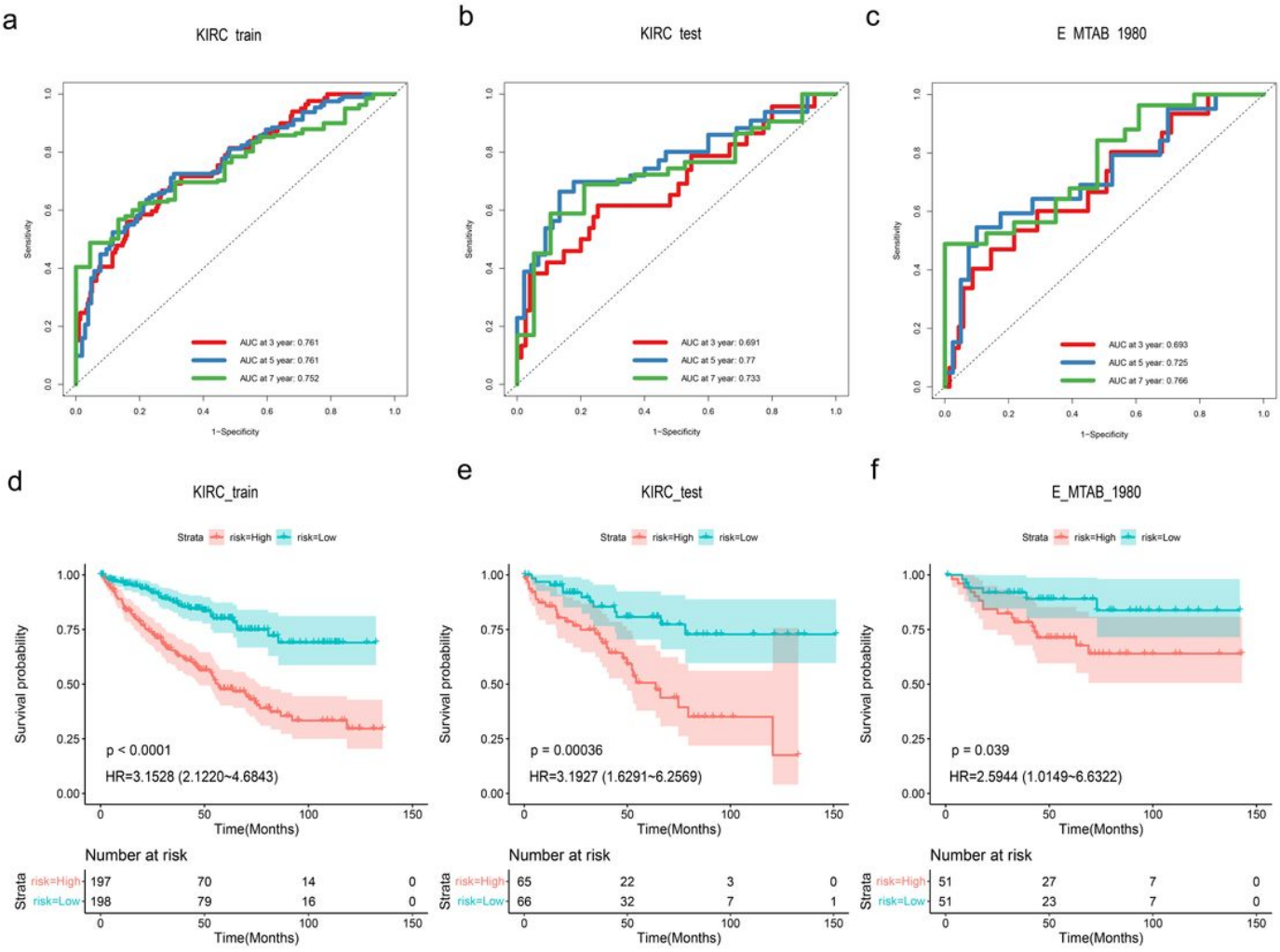


## Figure 2

The predictive accuracy of the prognostic model. (a-c) ROC curves analysis of the 3-, 5-, and 7-year in TCGA-KIRC train and test cohort as well as E-MTAB-1980 cohort respectively. (d-f) KM survival analysis of different risk groups in TCGA-KIRC train, test cohort and E-MTAB-1980 respectively

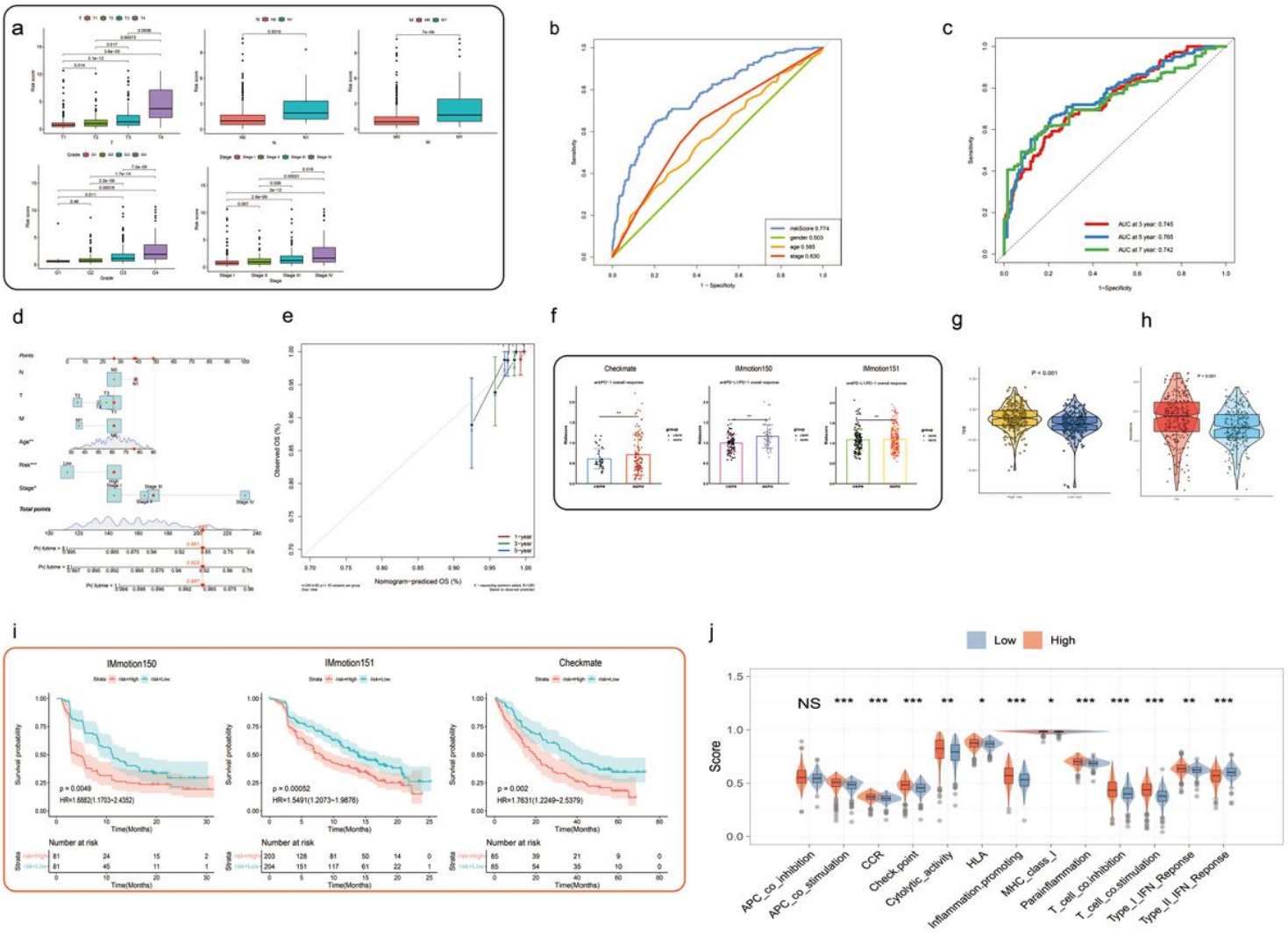


## Figure 3

Clinical features and a new nomogram as well as immunological characteristics. (a) Clinical correlation analysis in different risk groups of TCGA-KIRC. (b) ROC curves analysis of risk score and clinical information in TCGA-KIRC cohort. (c) ROC curves of OS in TCGA-KIRC cohort at 3 year, 5 years, and 7 years. (d) The nomogram to predict 1-, 3-, and 5-year OS in TCGA-KIRC cohort based on risk scores and clinical factors. (e) The Calibration chart for the evaluation of nomogram accuracy. (f) Differences of risk scores between CR/PR and SD/PD in the antiPD-L1/PD-1 overall response. (g) The violin plot for TIDE score in different risk groups. (h)The comparison of immune scores in different risk groups. (i) Role of the risk score in the immune function of TCGA-KIRC cohort.

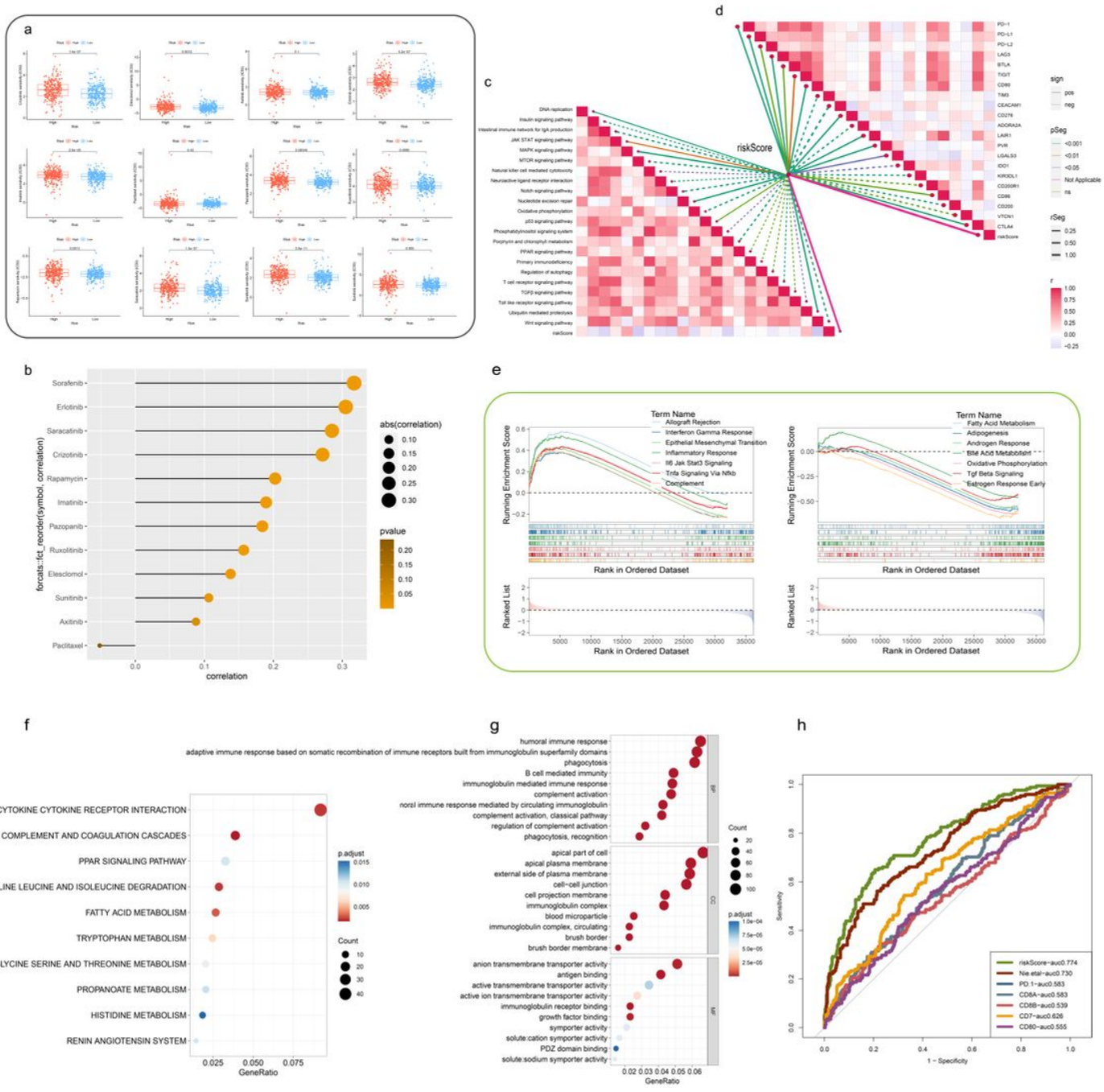


## Figure 4

Drug sensitivity analysis and identifying related pathways. (a) Identification of drug sensitivity between high-risk group and low-risk group. (b) Correlation of drug targets and risk score in TCGA-KIRC cohort. (c) Pearman's correlation analysis of functional pathways and risk score in TCGA-KIRC cohort. (d) Correlations between risk score and immune checkpoints. (e) Comparison of the enrichment of functional pathways by GSEA analysis of different related risk score. (f) KEGG enrichment of DEGs. (g)GO

enrichment analysis of the top 30 pathways in different risk groups. (h) The ROC curve of joint indicators and multi-model comparison.

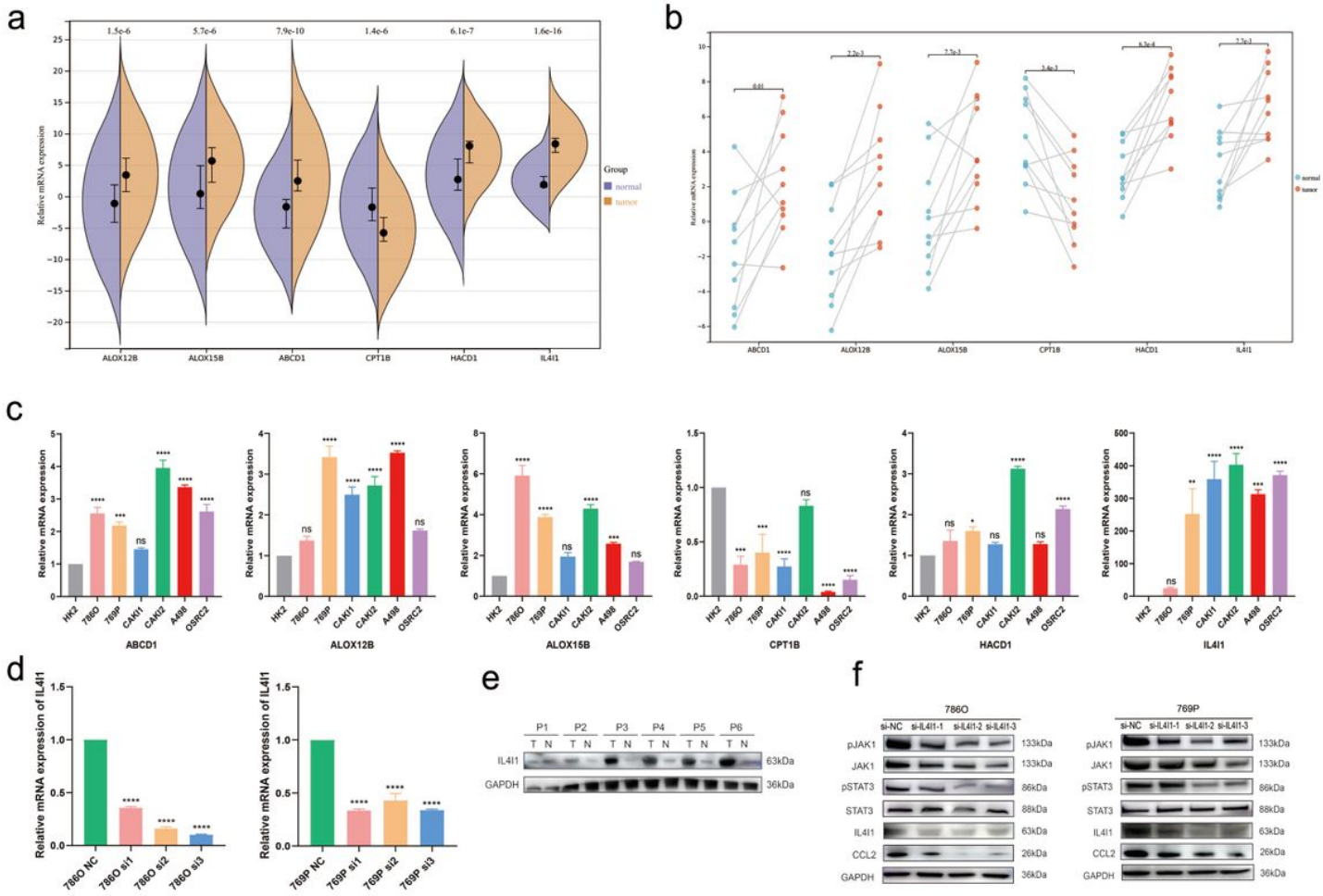


## Figure 5

Prediction and verification of expression levels of mRNA and protein. (a-c) mRNA expression of ABCD1, ALOX12B, ALOX15B, CPT1B, HACD1 and IL4I1 in different cell lines and normal as well as tumor samples. (d) Levels of the mRNA expression in si-IL4I1-transfected ccRCC cells (786-O and 769-P). (e) Protein expression of IL4I1 in ccRCC tumor tissue and normal tissues (f) Protein expression of IL4I1, JAK1, pJAK1, STAT3, pSTAT3, and CCL2 in si-IL4I1-transfected ccRCC cells (786-O and 769-P). *$P < 0.05$; ** $P < 0.01$; *** $P < 0.001$; **** $P < 0.001$.

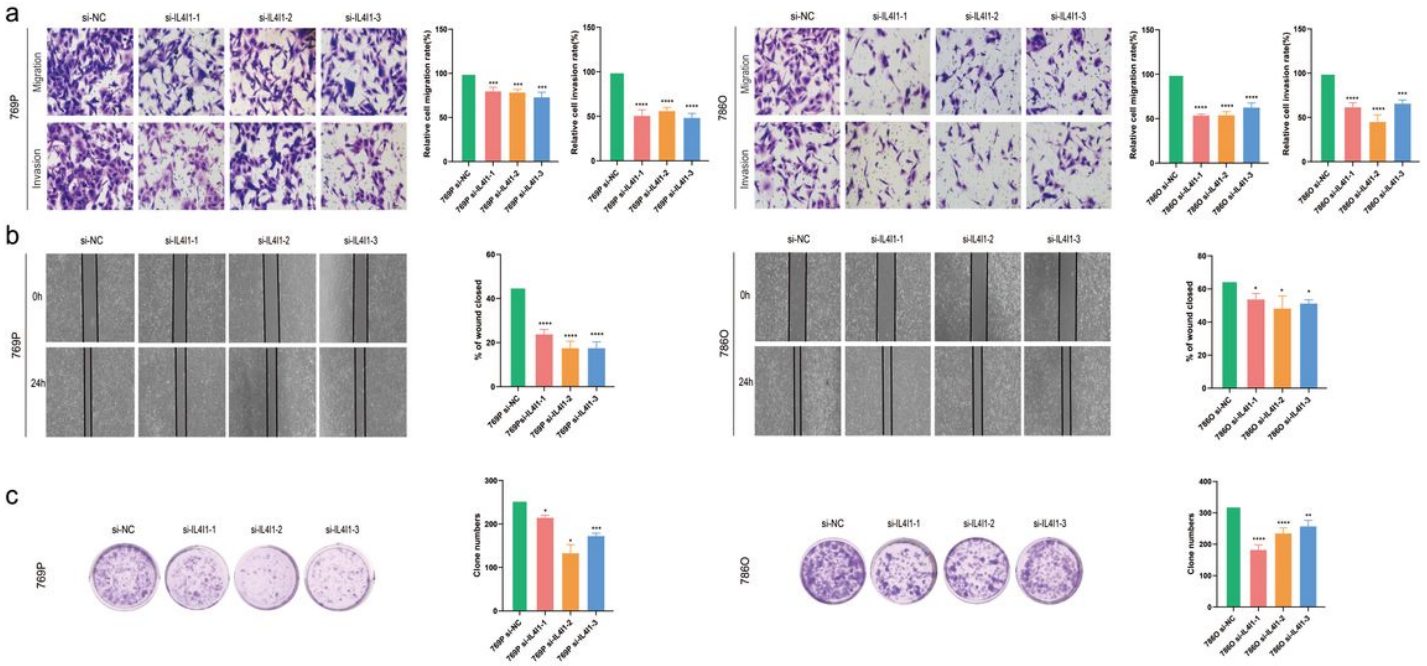


## Figure 6

Verification of IL4I1 for proliferation, migration, and invasion in ccRCC. (a) Transwell migration/invasion assay to analyse migration and invasion of ccRCC cell. (b-c) colony formation assays and wound healing to detect ccRCC cell proliferation. *$P < 0.05$; ** $P < 0.01$; *** $P < 0.001$; **** $P < 0.001$.

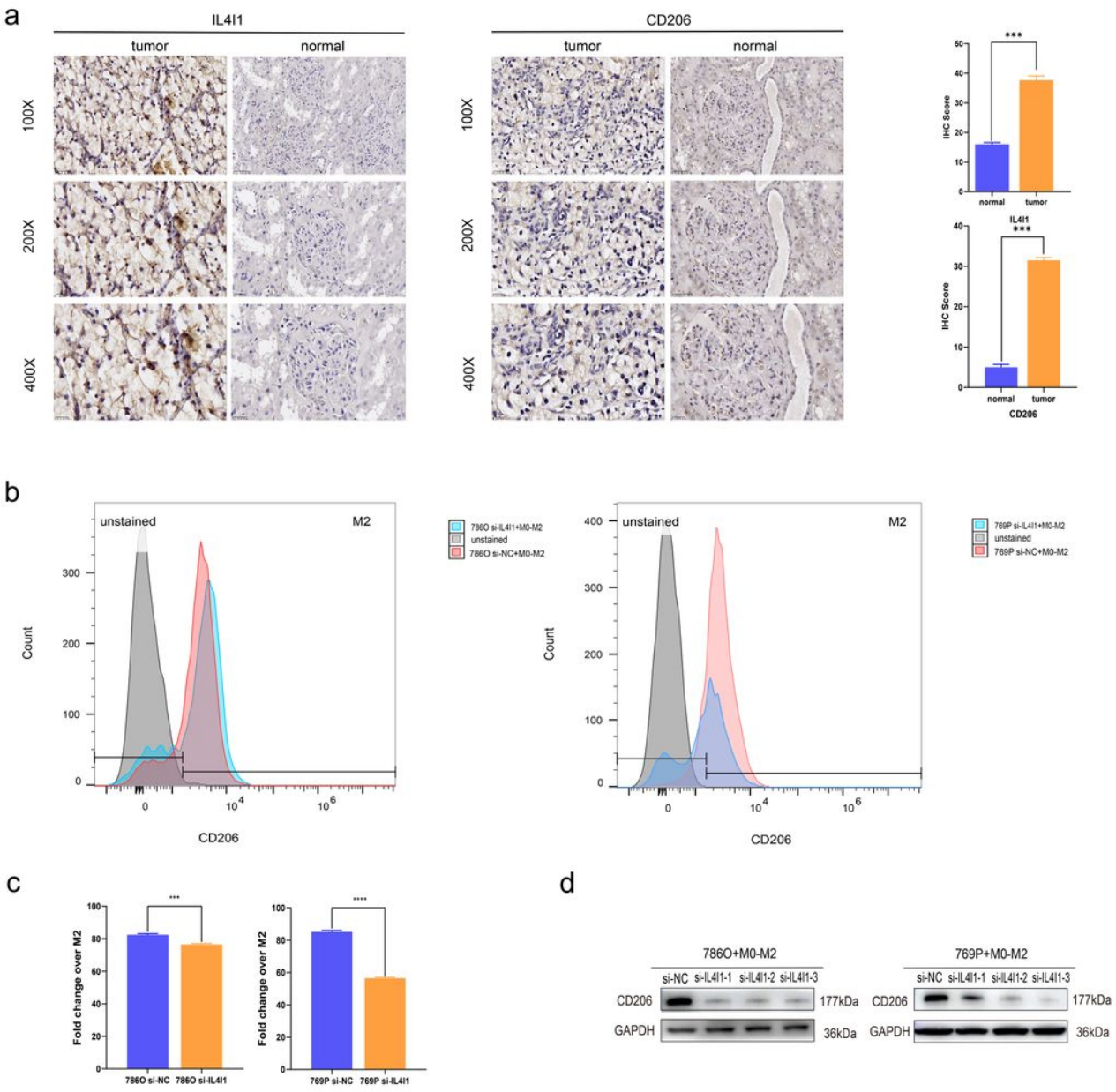


## Figure 7

Immunohistochemistry and Coculture assay. (a) Expression of IL4I1and CD206 in ccRCC tumor tissue and normal tissues by IHC. (b-c) Flow cytometry to detect M2-like macrophage polarization. (d) M2-like macrophage polarization after coculture assay conducted by western blot. *$P < 0.05$; ** $P < 0.01$; *** $P < 0.001$; **** $P < 0.001$.

# Supplementary Files

This is a list of supplementary files associated with this preprint. Click to download.

- TableS1.docx
- TableS2.docx
- TableS3.docx
- supplementaryFigures.docx